

## Wintertime cooling and a potential connection with transported aerosols in Hong Kong during recent decades

Xin Yang<sup>a,b</sup>, Chuanfeng Zhao<sup>a,b,\*</sup>, Lijing Zhou<sup>a</sup>, Zhanqing Li<sup>a,b,c</sup>, Maureen Cribb<sup>c</sup>, Sujuan Yang<sup>a</sup>

<sup>a</sup> State Key Laboratory of Earth Surface Processes and Resource Ecology, College of Global Change and Earth System Science, Beijing Normal University, Beijing, China

<sup>b</sup> Joint Center for Global Change Studies, Beijing, China

<sup>c</sup> ESSIC and Department of Atmospheric and Oceanic Science, University of Maryland, College Park, MD, USA



### ABSTRACT

As a southeast neighbor of the heavily industrialized and urbanized region of the Pearl River Delta (PRD), Hong Kong, China, has been susceptible to aerosols transported from the PRD in winter when the prevailing flow is from the west. The decadal trend in pollution during recent decades has likely indicated a difference in aerosol loading between winter and summer when different winds dominate. The surface air temperature shows a wintertime cooling trend during recent decades in Hong Kong, particularly during the midday hours. Differently, the surface air temperature shows a summertime warming trend during recent decades in Hong Kong. By examining the distinct winter versus summer trends in midday hour temperature under low cloud cover conditions in Hong Kong from 1979 to 2014, we found a close relationship between the temperature reduction during midday hours and increased aerosol loading in winter but not in summer. The consistency in turning point for both the increase in aerosol loading and the variation in winter-summer temperature differences in the late 1980s also supports the strong association between aerosol and temperature changes. Further analysis shows that there was a significant negative correlation between downwelling solar radiation (DSR) and aerosol loading. Quantitatively, aerosols over Hong Kong during the study period reduced surface DSR and midday temperatures by approximately  $30 \text{ W m}^{-2}$  and  $2.1^\circ\text{C}$  for low cloud cover cases.

### 1. Introduction

A decreasing trend in surface solar radiation during recent decades has been reported over many regions in China (Qian et al., 2003, 2007; Che et al., 2005; Shi et al., 2008). Regions with reduced downwelling solar radiation (DSR) have often had heavy aerosol loading, pointing to the effect of aerosols on surface DSR (Li, 1998; Li et al., 2007, 2010; Cao et al., 2006; Xia et al., 2006; Cao et al., 2007; Tang et al., 2011; Wang et al., 2015). The reduction of DSR by aerosols cools the surface and weakens the vertical turbulence, slowing surface winds subsequently (Jacobson and Kaufman, 2006; Yang et al., 2013a). The reduction of surface DSR can also prevent the vertical development of the boundary layer (Quan et al., 2013, 2014; Du et al., 2013; Li et al., 2017). These effects of aerosols on surface DSR and winds near surface can further increase the particulate mass concentration by confining aerosols to a lowered boundary layer (Dong et al., 2017). Higher aerosol concentration in turn blocks solar radiation more effectively and intensifies the reduction of surface DSR more efficiently (Yang et al., 2016a). The decrease in surface DSR caused by aerosol pollutants has contributed

significantly to temperature decreases in China (Liu et al., 2004; Wang and Dickinson, 2013; Li et al., 2016a). The land surface is heated by DSR and this heat is transferred to the overlying air. Near-surface air temperatures then rise, gradually reach a maximum value in the early afternoon. This is the physical relationship between DSR and air temperature during daytime hours. The reduction in daily maximum temperature ( $T_{\max}$ ) caused by reduced surface solar radiation has been reported in many regions (Liu et al., 2004; Makowski et al., 2009) and an association with anthropogenic aerosols has been proposed (Wild et al., 2007). Based on model simulations, Qian and Giorgi (2000) suggested a connection between observed declining temperature trends and increasing anthropogenic aerosol loading in China. The lack of warming so far this century has been attributed to surface cooling effects by aerosol pollution, especially in Asia where aerosol emissions have grown rapidly (Wild et al., 2007; Kaufmann et al., 2011; IPCC, 2013; Wang et al., 2015).

Few studies have examined the cooling contribution of aerosol pollution to the temperature variability on a decadal timescale as well as the competing warming effects by greenhouse gases (GHGs) (Yang

\* Corresponding author at: State Key Laboratory of Earth Surface Processes and Resource Ecology, College of Global Change and Earth System Science, Beijing Normal University, Beijing, China.

E-mail address: [czhao@bnu.edu.cn](mailto:czhao@bnu.edu.cn) (C. Zhao).

et al., 2013a). As a close neighbor of the Pearl River Delta (PRD) region, Hong Kong has been subject to air pollution transported from the west in recent decades, which is especially heavy in winter due to the northwest monsoon wind in the region (Yuan et al., 2006; Jiang et al., 2007; Deng et al., 2008; Garland et al., 2008; Li et al., 2016a, 2016b). By comparing aerosol loading, temperature variations, and related meteorological factors between summer and winter in Hong Kong, this study investigates the possible relationship between midday surface air temperature and aerosol amount on a decadal timescale. We then examine the hypothesis that variations in pollution aerosols are an important contributing factor to local climate change, including the observed cessation of warming during the last 10 years.

## 2. Dataset and methodology

It is challenging to distinguish the impacts of aerosols on near-surface temperature from those of GHGs, urban heat islands, and natural variability. Examining the daily maximum changes in near-surface air temperature is one approach to investigate aerosol surface cooling effects (Gong et al., 2006; Yang et al., 2013a). This approach strongly limits the influence from GHGs and urban heat islands since their effects have a weak diurnal variation. The effect of aerosols on near-surface air temperature has a strong diurnal variation. Besides, Yang et al. (2013a) took advantage of the topography of mountain and plain and found that aerosol cooling is much more evident in the plain than in the nearby mountain. The contrast is a sound indicator of the aerosol cooling effect whose long-term trends also differ considerably between the two locations, which has little to do with the greenhouse effect.

In this paper, we examine the decadal changes in diurnal temperature cycles to explore aerosol impacts on temperature. The study region and locations of the stations are shown in Fig. 1a. The longest continuous dataset for hourly temperature obtained from NOAA's National Climatic Data Center (<ftp://ftp.ncdc.noaa.gov/pub/data/noaa/>) covers 1979 to 2014, although observations started in 1950s. Limited by the availability of datasets, four nine-year periods (1979 to 2014) of observations of hourly near-surface air temperature, horizontal atmospheric visibility (VIS), relative humidity (RH), winds, and clouds at the Hong Kong Observatory were used to examine the variation in temperature with respect to aerosol loading. Other data used in this study include particulate matter with aerodynamic diameters  $< 2.5 \mu\text{m}$  (PM<sub>2.5</sub>, and surface DSR). DSR data are only available from 2009 to 2014. PM<sub>2.5</sub> mass concentrations have been measured since 1999 at Central station of Hong Kong by the Environmental Protection Department of Hong Kong (<http://epic.epd.gov.hk/EPICDI/air/station/>). To analyze the relationship between DSR and aerosol loading, PM<sub>2.5</sub> and VIS data from 2009 to 2014 were used in this study. The impact of RH on VIS was largely reduced by using the equivalent visibility under dry conditions (VIS(dry)) when RH was  $> 40\%$  (Rosenfeld et al., 2007). The correction formula is expressed as  $\text{VIS}/\text{VIS}(\text{dry}) = 0.26 + 0.4285 \log(RH \times 100)$ . This correction formula is first put forward by Rosenfeld et al. (2007) and has since been extensively used to study aerosol effects in many regions across China including PRD region (Qian et al., 2009; Yang et al., 2013a, 2013b; Yang et al., 2016a, 2016b). This RH-corrected visibility is not always more than the measured visibility, such as the cases when  $RH > 40\%$  and  $RH < 46\%$  (Yang et al., 2016a). RH-corrected visibility has been widely used in previous studies (Wang et al., 2009; Yang et al., 2013b; Yang et al., 2016a, 2016b). According to the weather record, instances of fog and precipitation were excluded from the visibility trend analysis.

Fig. 1b and c show the different prevailing winds between summer and winter in the monsoon climate of Hong Kong. Stemming from the nearby west Pacific Ocean surface, moist and clean summer air contributes to more frequent precipitation and thus more efficient aerosol wet deposition. By contrast, stronger westerly winter winds transport more aerosols from the upwind of the western PRD region, leading to more aerosols in winter than in summer. The contrast in aerosol

concentration has also been reported in other studies (Yuan et al., 2006b; Li et al., 2016a, 2016b).

Fig. 2a further shows the different temporal trends in aerosol loading in summer and winter inferred from atmospheric visibility in Hong Kong, which is presumably associated with different aerosol sources caused by the shift in prevailing winds as demonstrated in Fig. 1b and c. As the source region of aerosol loading, Pearl River Delta megacity area of Guangdong had experienced a steady increase in pollution emission (Wu et al., 2005; Deng et al., 2008; Wang et al., 2011) until a few years ago when air quality began to improve (Tao et al., 2015). According to Fig. 2a, summertime visibility is much better than wintertime visibility and this distinct seasonal difference has an increasing trend with time. Similarly, the temporal variations of daily PM<sub>2.5</sub> in Fig. 2b also suggest the large difference between summer and winter in Hong Kong. This allows us to examine the impacts of aerosol concentration on near-surface temperature and surface DSR. Note that atmospheric visibility instead of PM<sub>2.5</sub> is used in this study due to the fact that PM<sub>2.5</sub> observations are not available until 1999. Instead, we examined the relationship between PM<sub>2.5</sub> and atmospheric visibility in both summer and winter over Hong Kong since 1999, shown in Fig. 2c and d. They are closely correlated, which indicates that atmospheric visibility could serve as valid proxy for aerosol loading. Similar relationships have also been found by Yang et al. (2016b).

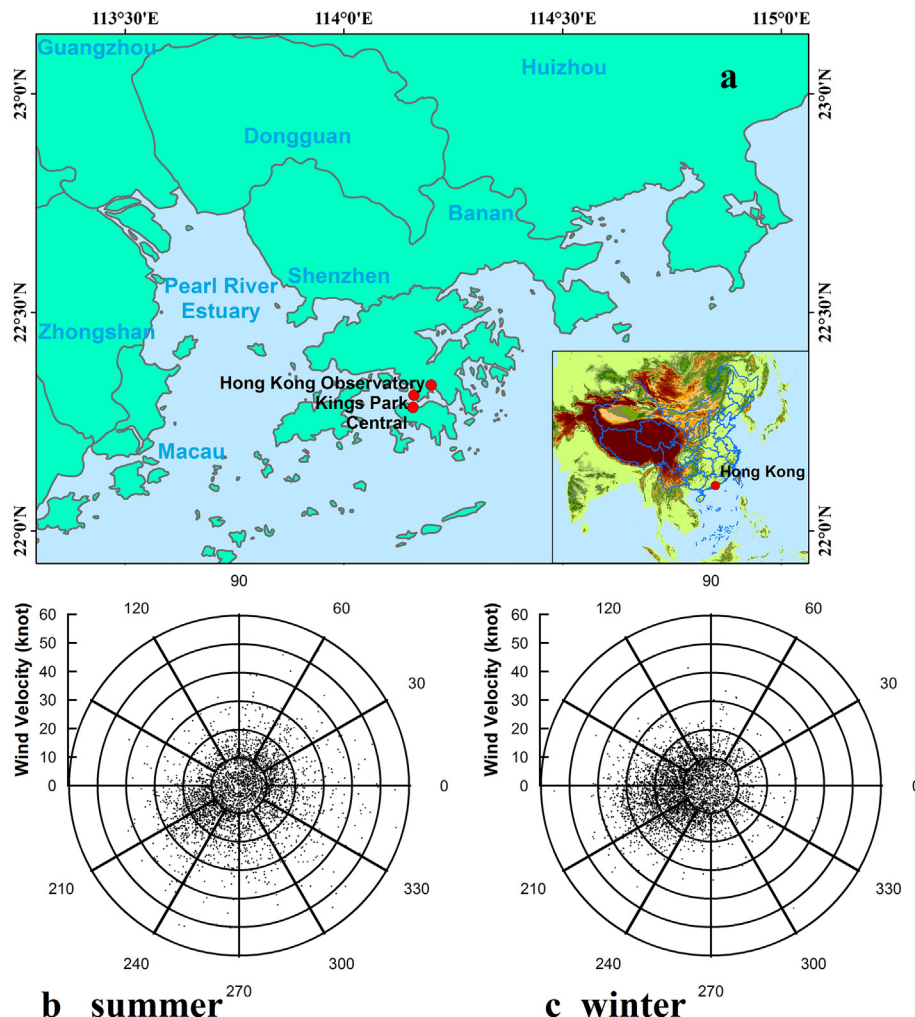
The cloud cover is estimated by an observer on the roof of the Hong Kong Observatory Headquarters building, an open area from where the whole sky can be seen. Dividing the whole sky into eight equal parts, the observer estimates the proportion of the sky covered by clouds. For example, the cloud cover is recorded as "8/8" or 100% when the whole sky is covered by clouds and the cloud cover is recorded as "4/8" or 50% when half of the sky is covered by clouds. Criteria used to estimate nine specific cloud cover values (0%, 13%, 25%, 38%, 50%, 63%, 75%, 88%, and 100%) are shown in Table 1. Considering that completely clear skies (cloud fraction = 0%) are rare in Hong Kong, especially during summer, we conducted the analysis for low cloud cover (0%, 13%, 25%), and high cloud cover (75%, 88%, 100%) scenarios, respectively. This rough classification according to cloud cover helps to limit the influence of clouds on surface radiation and to ensure sufficient data samples in the analysis.

## 3. Results and discussion

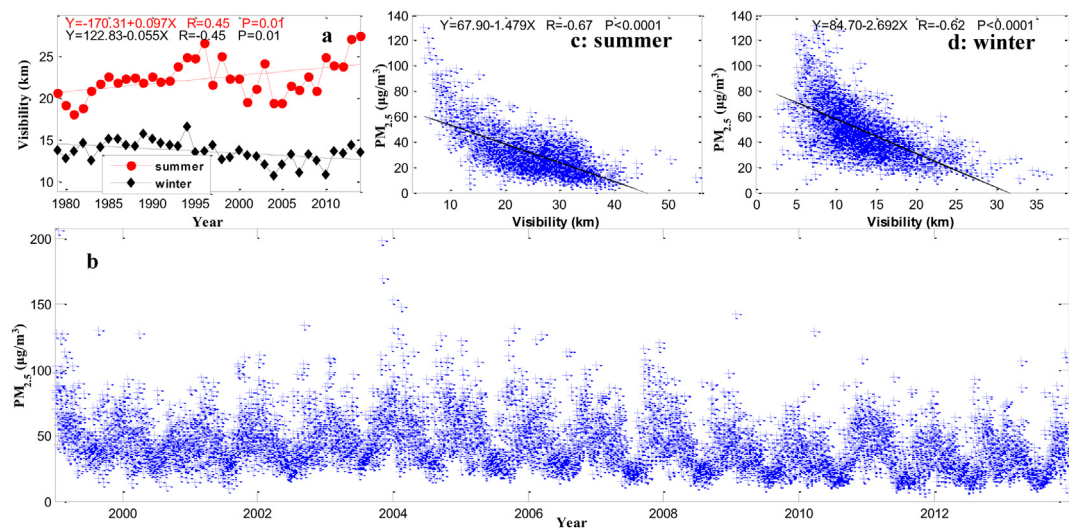
### 3.1. Distinct temperature trends between summer and winter

Fig. 3 shows the diurnal variation in average temperature during four nine-year periods (1979–1987, 1988–1996, 1997–2005, and 2006–2014) in both summer and winter months (June to September and November to February, respectively) for low cloud cover and high cloud cover scenarios. The increasing trend in summer temperature in Hong Kong is significant for all time. When the cloud cover is high (Fig. 3b), the rise in near-surface air temperatures in each of the four nine-year periods is evenly distributed throughout the day, while under low cloud cover scenarios (Fig. 3a), the midday temperature increase is larger in magnitude compared to other times of the day. More clouds seem to reduce daily maximum temperature ( $T_{\max}$ ) but do not change the temporal increasing variation of average temperature in summer seen over the past few decades. Temporal changes in average temperature are similar for both cloud cover scenarios. The general increasing trend in summer average temperature in Hong Kong is consistent with the widespread rise in surface temperature across China, which has been largely attributed to the buildup of GHGs (Meehl et al., 2003; IPCC, 2013). The observed gradual warming trend during the summers of 1979–2014 in Hong Kong also agrees well with changes in global mean surface temperature during the past three decades, each of which has been successively warmer than any preceding decade since 1850 (IPCC, 2013).

Although global mean surface temperatures continue to rise, the



**Fig. 1.** (a) Location of the study area, i.e., Hong Kong in southeast China. Locations of the Hong Kong Observatory, the PM<sub>2.5</sub> observation station in Central, and the Kings Park radiosonde station are also shown on the map. Distributions of wind speed (knot, 1 knot = 0.5144 m s<sup>-1</sup>) and direction (degrees azimuth) in Hong Kong in (b) summer and (c) winter. Each point in panels (b) and (c) represents the mean 700–800 hPa wind vector at 2000 Local Time.



**Fig. 2.** (a) Temporal variations in seasonally-averaged equivalent visibility at Hong Kong during the summer (June–July–August–September, in red) and winter (November–December–January–February, in black) seasons of 1979–2014. (b) Temporal variations in the daily averaged PM<sub>2.5</sub> during the period of 1999–2014. (c) Scatter plot of hourly equivalent visibility and PM<sub>2.5</sub> at Hong Kong during the summer (June–July–August–September) seasons of 1999–2014. (d) The same as (c) but for winter season. (For interpretation of the references to colour in this figure legend, the reader is referred to the web version of this article.)

**Table 1**  
Criteria for estimating cloud cover.

Cloud Cover	0%	1/8 ≈ 13%	2/8 = 25%	3/8 ≈ 38%	4/8 = 50%	5/8 ≈ 63%	6/8 = 75%	7/8 ≈ 88%	8/8 = 100%	9/8
Description	Clear	Almost clear	Nearly clear	Sparingly cloudy	Partly cloudy	Broken cloudy	Thick cloudy	Cloud covers almost the whole sky	Cloud covers the whole sky	Cannot observe
Symbol	○	○ ⊖	○ ⊖ ⊖	○ ⊖ ⊖ ⊖	○ ⊖ ⊖ ⊖ ⊖	○ ⊖ ⊖ ⊖ ⊖ ⊖	○ ⊖ ⊖ ⊖ ⊖ ⊖ ⊖	○ ⊖ ⊖ ⊖ ⊖ ⊖ ⊖ ⊖	○ ⊖ ⊖ ⊖ ⊖ ⊖ ⊖ ⊖ ⊖	○ ⊖ ⊖ ⊖ ⊖ ⊖ ⊖ ⊖ ⊖ ⊖

warming trend might be compromised by the cooling effect of anthropogenic aerosols at certain locations or regions (Jacobson and Kaufman, 2006; Huang et al., 2007; Yang et al., 2013a). Associated with the location and monsoon climate background, aerosol loading in Hong Kong is much higher in winter than in summer. Fig. 2 shows the clear difference in both the magnitude and trend in RH-corrected visibility between winter and summer. Aerosol loading in winter is greater than in summer and the difference between them has increased with time during the last four decades, except for the last few years when visibility has improved somewhat thanks to the exceptional effort in combating air pollution in China with the most dramatic changes in the Pearl Delta Region (Zhao et al., 2013; Wang et al., 2014). Winter temperatures in Hong Kong are therefore more susceptible to aerosol surface cooling effects. Similar results have also been found by using uncorrected atmospheric visibility data, which is not shown here. As shown in Fig. 3d, the rise in winter temperature for the low cloud cover scenario during the second nine-year period (1988–1996) compared to that during the first period (1979–1987) is  $\sim 2^{\circ}\text{C}$ , which is much larger than the summer warming ( $< 1^{\circ}\text{C}$ ) during the same period. This seasonal characteristic of warming is consistent with the reported temporal heterogeneity in GHG-induced warming, which is most significant in winter, followed by spring, fall, and summer (IPCC, 2013). However,

this winter warming for the low cloud cover scenario has ceased since the second nine-year period, i.e.,  $T_{\max}$  in winter have fallen since the second nine-year period. For the other hours of the day, winter warming lasted until the third nine-year period, i.e., temperatures started to decrease only in the last nine-year period (2006–2014). Midday near-surface air temperatures during the last nine-year period are lower than that during the first nine-year period for the low cloud cover scenario in winter. This decreasing temperature trend is only seen for the low cloud cover scenario in winter. Winter warming for the high cloud cover scenario lasted throughout the four nine-year periods (Fig. 3e). The variation in temperature for the high cloud cover scenario is similar in winter to that in summer when the warming is evenly distributed between day and night. All-sky average wintertime temperatures during midday hours change in a similar way as those for the low cloud cover scenario, while the average wintertime temperature variation at other hours of the day is more like that for the high cloud cover scenario (Fig. 3f). These comprehensive changes in near-surface air temperatures indicate that air temperatures at midday hours are more sensitive to the effects of clouds and aerosols because there is more solar shortwave radiation arriving from space at this time. Near-surface air temperatures at other hours of the day are more controlled by longwave radiation, which is more sensitive to the influence of GHGs

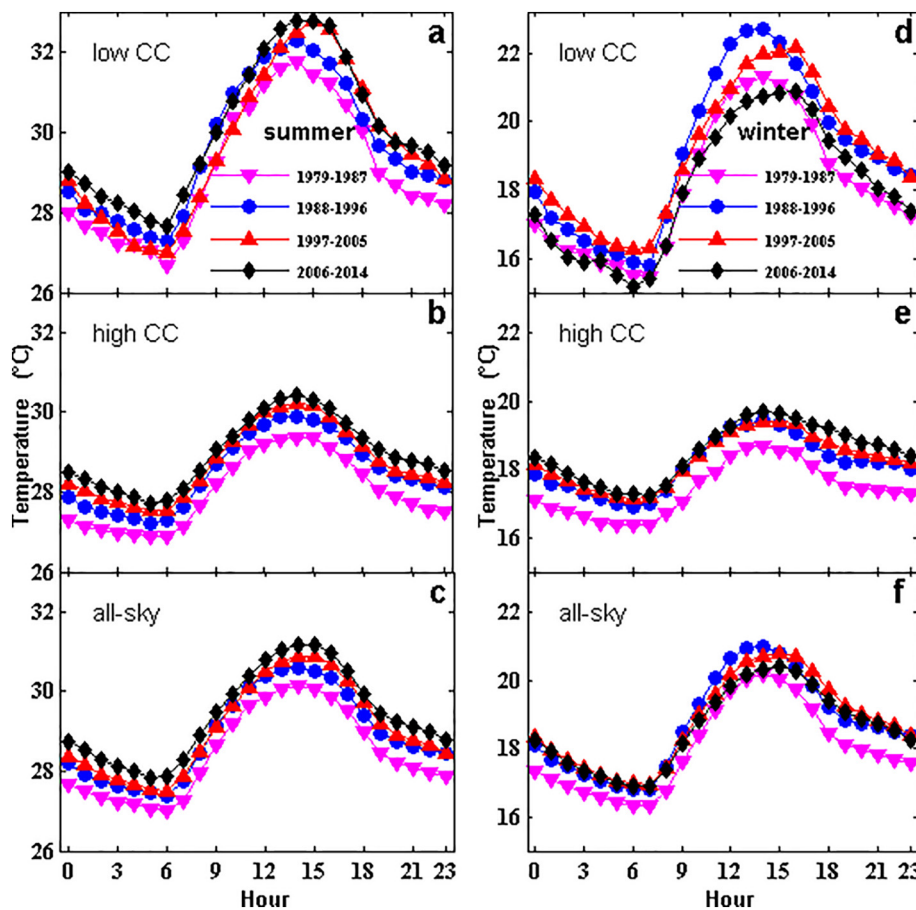


**Fig. 3.** Diurnal variations in average temperature for the four nine-year periods in Hong Kong. Panels (a) to (c) show results for low cloud cover (CC), high CC, and all-sky scenarios, respectively, in the summer (June–July–August–September). Panels (d) to (f) show results for low CC, high CC, and all-sky scenarios, respectively, in the winter (November–December–January–February). The four nine-year periods are: 1979–1987 (magenta), 1988–1996 (blue), 1997–2005 (red), and 2006–2014 (black). Low, and high CCs are defined as 0–25%, and 75–100%, respectively. The time is local time. For all the changes among the four nine-year periods, the difference in midday hours (1000–1600 Local) temperature for low CC scenarios is statistically significant at the 0.05 level based upon a Student's t-test. Other temperature changes in midday pass the Student's t significant test at 0.05 level expect for the changes between 1988 and 1996 and 1997–2005 for low CC scenario in summer, high CC scenario in winter and all-sky scenario in winter. (For interpretation of the references to colour in this figure legend, the reader is referred to the web version of this article.)

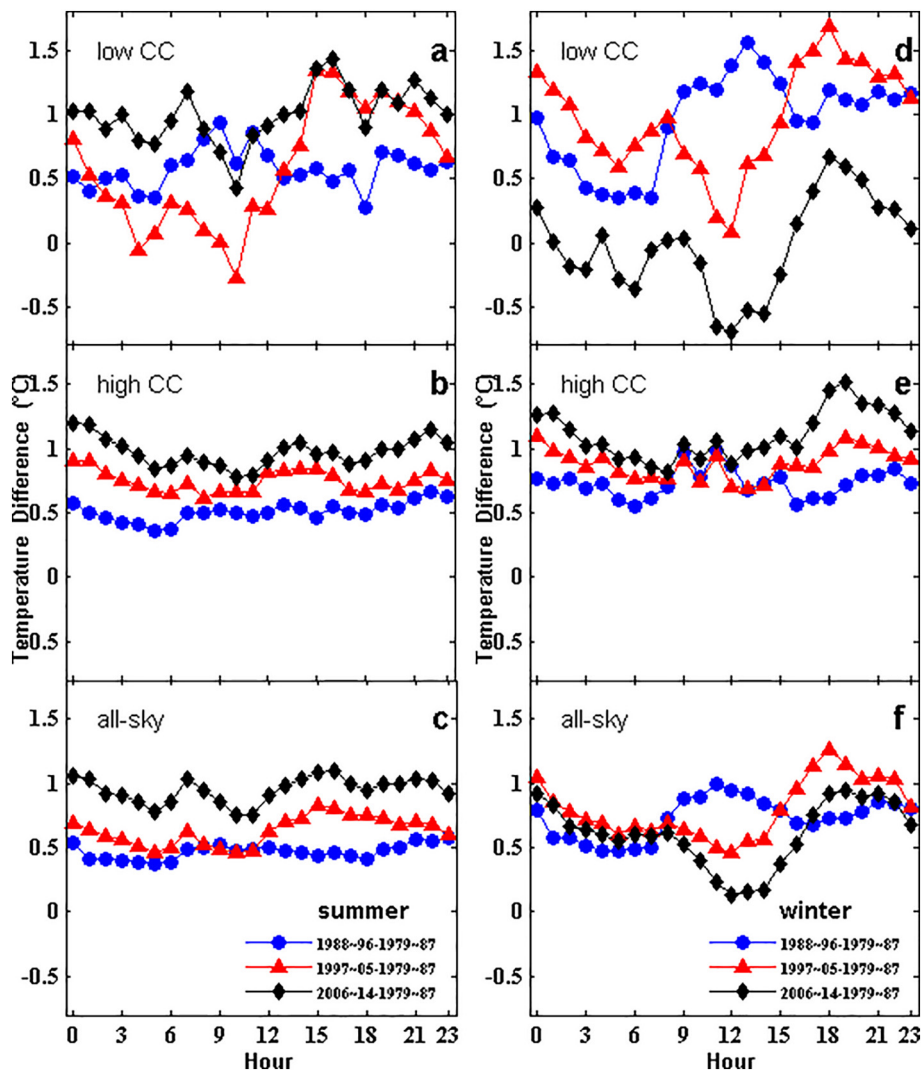


**Fig. 4.** Same as Fig. 3, but for the relative change in average temperature diurnal variations of the last three nine-year periods with respect to the first nine-year period in Hong Kong. The periods shown are: 1988–1996 (blue), 1997–2005 (red), and 2006–2014 (black) with respect to 1979–1987. (For interpretation of the references to colour in this figure legend, the reader is referred to the web version of this article.)

and cloud bases (Garrett and Zhao, 2006; Zhao and Garrett, 2015).

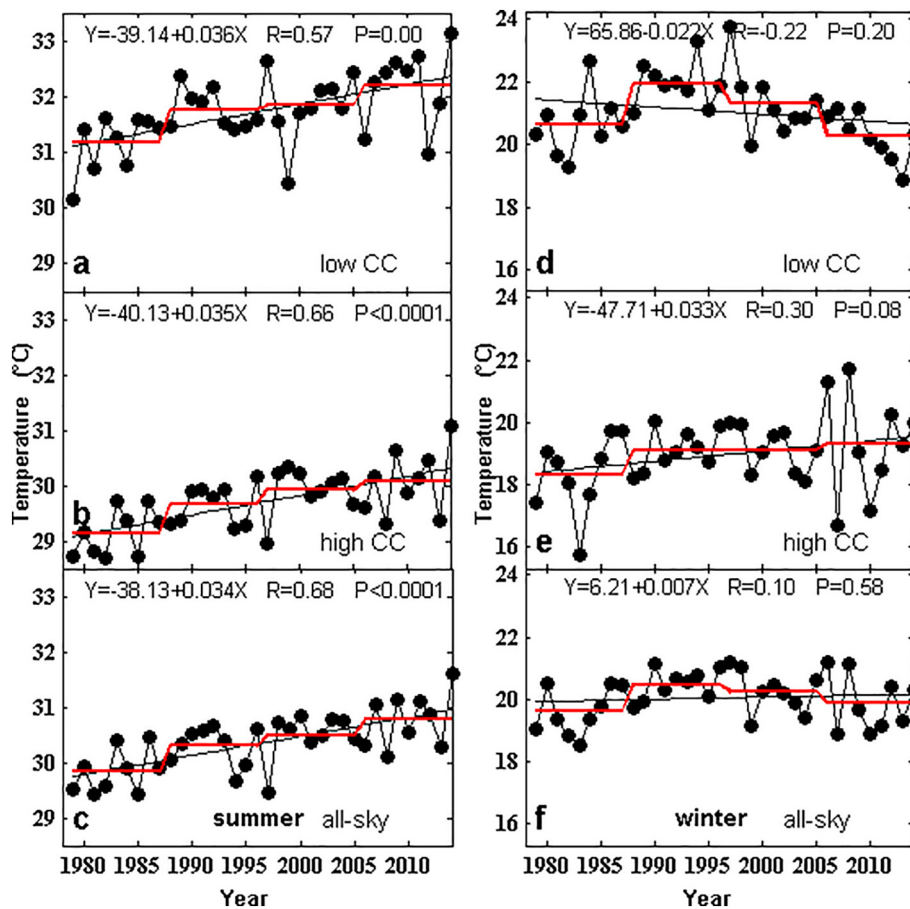
Fig. 4 shows the diurnal variation in relative temperature change during the last three nine-year periods with respect to the first nine-year period. The changes are almost all positive in summer for the two cloud cover scenarios (Figs. 4a–c) and in winter for the high cloud cover scenario (Fig. 4e), confirming a similar fundamental warming trend during the two seasons. By contrast, winter temperatures for the low cloud scenarios show a clear drop during midday hours in the last nine-year period (Fig. 4d). Fig. 4f shows that the winter temperature change for the all-sky scenario is similar to that for the all-sky scenario in summer except for midday (Fig. 4c), suggesting the dominating influence of aerosols on winter temperature during midday.

Fig. 5 shows the temporal variation in seasonally-averaged midday (10:00 Local Time, or LT, to 16:00 LT) temperatures in Hong Kong from 1979 to 2014. Midday temperatures in summer show a significant upward trend for all two cloud cover scenarios and the all-sky scenario (Fig. 5a–c). The correlation coefficient  $R$  is  $> 0.5$  for the temporal trend of temperature in Fig. 5a–c, indicating the midday warming is significant. Similarly,  $P$  value is all below 0.01 for Fig. 5a–c, suggesting the warming trend passes the 95% confidence significance test. But in winter (Fig. 5d–f), midday temperatures for all but the high cloud cover scenario (Fig. 5e) show a strong cooling shift starting from the beginning of the third nine-year period (1997). These changes are consistent

with the decadal changes in the diurnal variation of temperature shown in Fig. 3.

### 3.2. Possible links between temperature variation and aerosol cooling effects

The distinct trends in temperature between summer and winter in Hong Kong presented in Section 3.1 are closely linked to the different aerosol loadings in several ways. First, the turning point seen in both the increase in aerosol loading (represented by visibility in Fig. 2) and the opposite changes in temperature between summer and winter in Hong Kong (Figs. 3, 4, and 5) in the late 1980s are consistent. The PRD region upwind of Hong Kong has experienced heavy aerosol emissions accompanied by rapid economic growth during recent decades (Andreae et al., 2008; Garland et al., 2008). Stronger northwesterly winter winds transport substantially more aerosols from the upwind PRD region than southeast summer winds. Consequently, the heavy aerosol loading since the late 1980s could have substantially cooled the surface in winter in Hong Kong, causing a clear winter temperature reduction after the late 1980s (Figs. 3, 4, and 5). One thing we should note is that the winter time cooling trend keeps in the period from 2000 to 2010 (Fig. 5d), while the atmospheric visibility ( $\text{PM}_{2.5}$ ) only shows clear decreasing (increasing) trend till 2004 and no clear (slight decreasing) temporal trend from 2004 to 2010. This could result from



**Fig. 5.** Annual variations in daily-averaged (1000–1600 Local Time) temperature in Hong Kong. Panels (a) to (c) show results for low cloud cover (CC), high CC, and all-sky scenarios, respectively, in the summer (June–July–August–September). Panels (d) to (f) show results for low CC, high CC, and all-sky scenarios, respectively, in the winter (November–December–January–February). Low, and high CCs are defined as 0–25%, and 75–100%, respectively. The black line through the points is the linear best-fit line. Connecting red lines show the trends in each of the four nine-year periods. (For interpretation of the references to colour in this figure legend, the reader is referred to the web version of this article.)

uncertainties associated with the vertical distribution of aerosol particles, the variation of boundary layer height and relative humidity, the aerosol types, and so on. By contrast, the increasing trend of visibility in summer should also contribute to the summer warming trend throughout the study period, along with the GHGs warming effect. Thus, the large difference in temporal variations of atmospheric visibility between summer and winter in Hong Kong, could help explain the corresponding differences in temporal variations of near surface temperature.

Second, the diurnal cycle of the winter temperature reduction in Hong Kong seems consistent with the aerosol radiative effects: the strong reduction in temperature occurs at midday hours when the aerosol cooling effect is the strongest. According to the temperature changes for both the low cloud cover scenarios shown in Fig. 3d, winter cooling in the last two nine-year periods (1997–2005 and 2006–2014), compared to the second nine-year period (1988–1996), occurred during the day time only. Another noticeable feature is that there is a delay in the time of occurrence of the  $T_{\max}$  in winter for low cloud cover scenario: 14:00 LT during the first two nine-year periods versus 16:00 LT during the last two nine-year periods. The delay in the time of occurrence of  $T_{\max}$  in winter may be related to the interaction and feedback between aerosols and radiation. Summertime temperatures continuously rise at a nearly uniform rate during the day and night. These distinguishing features in the changes in diurnal temperature variation suggest that aerosol negative radiative forcing is the most likely cause for the winter temperature decrease in recent decades in Hong Kong.

The observed surface cooling associated with aerosol loading in Hong Kong is similar to that in the Sichuan Basin, the Guanzhong Plain, and East Asia (Qian and Giorgi, 2000; Kim et al., 2010; Yang et al., 2011, 2013a; He et al., 2013). Surface cooling related to aerosols is usually reported in the summer for most regions but is observed in

winter in Hong Kong. This is associated with the uneven distribution of aerosol pollution in space and time. Aerosol emissions directly reduce the surface radiation and consequently the regional temperature in many regions (He et al., 2013; Wu et al., 2015; Yang et al., 2016a, 2016b). In Hong Kong, surface DSR for the low cloud cover scenario is also significantly correlated with summertime and wintertime aerosol loading (Fig. 6a-d). The sensitivities of surface DSR to RH-corrected visibility for the low cloud cover scenario are 12.63 and 15.08  $\text{W m}^{-2} \text{km}^{-1}$  in summer and winter, respectively. The sensitivity of surface DSR to RH-corrected visibility in winter time is similar to the value of 15.42  $\text{W m}^{-2} \text{km}^{-1}$  found in Beijing in November 2014 in a study that did not consider the impact of clouds (Yang et al., 2016a). The linear sensitivities of surface DSR to  $\text{PM}_{2.5}$  are 7.49 and 5.12  $\text{W m}^{-2} \mu\text{g}^{-1} \text{m}^{-3}$  for the low cloud cover scenario in summer and winter, respectively. Fig. 6e-h is the same as Fig. 6a-d except that a logarithmic scale is used for the x-axes. This is done to remove the effects of the difference in units between visibility and  $\text{PM}_{2.5}$ . The magnitudes of the slopes for both aerosol loading proxies are similar when using a logarithmic scale, especially in winter, i.e., 561.00 for using visibility and 535.19 for using  $\text{PM}_{2.5}$ . This shows that both atmospheric visibility (Fig. 2) and  $\text{PM}_{2.5}$  can be used to represent aerosol loading in this study.

Fig. 7 shows monthly mean near-surface air temperature as a function of the total surface DSR from 10:00–16:00 LT under low cloud cover condition in Hong Kong. As expected, a significant increasing trend in near-surface air temperature as the surface DSR increases is seen in both summer and winter under low cloud cover conditions. Note that the daily DSR from 10:00–16:00 LT in Fig. 7 is the average of the total DSR during these hours, which makes the daily DSR sometimes higher in winter than in summer. According to the results shown in Fig. 6, surface DSR decreases as aerosol loading increases, i.e., if

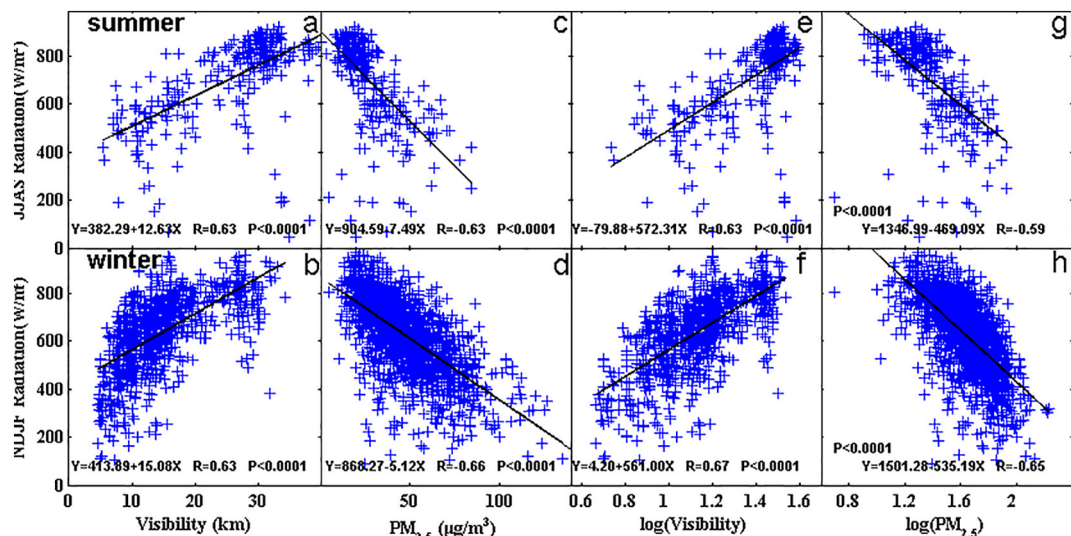


**Fig. 6.** Hourly mean surface downwelling solar radiation as a function of hourly mean visibility (panels a and b) and  $\text{PM}_{2.5}$  (panels c and d) for the low cloud cover (0–25%) scenario. Hourly averages during the day are calculated from 1000 to 1600 Local Time. Panels (e) and (f) are the same as (a) and (b) except that the x-axes are now logarithmic. Panels (g) and (h) are the same as (c) and (d) except that the x-axes are also now logarithmic. The top panels are for summer and the bottom panels are for winter.

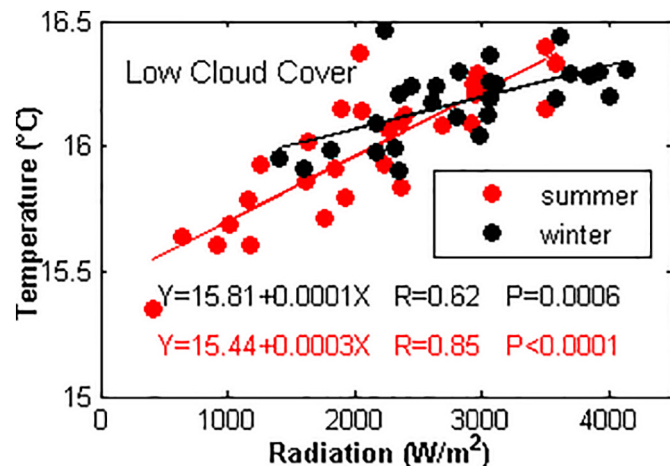


**Fig. 7.** Monthly mean temperature as a function of surface direct downwelling solar radiation for the low cloud cover (0–25%) scenario in summer (red) and winter (black). Averages during the day are calculated from 1000 to 1600 Local Time. (For interpretation of the references to colour in this figure legend, the reader is referred to the web version of this article.)

visibility decreases or  $\text{PM } 2.5$  increases. As a consequence, the near-surface air temperature also decreases (Fig. 7). This reasonable link between the temperature decrease and the aerosol surface cooling effect explains well the reduction of temperature drop and increase of pollution during winter in Hong Kong.

### 3.3. Variations in cloud cover

During the past several decades, total cloud fraction has significantly decreased over much of China, including the PRD region adjacent to Hong Kong (Kaiser and Qian, 2002; Qian et al., 2006; Xia, 2012). It is necessary to examine if the variation in cloud fraction is responsible for the temperature trend seen in Figs. 3 and 5. Considering that both the wintertime temperature decrease and the possible surface cooling effect by aerosols are strongest at midday, we examined the variation in cloud cover from 10:00 LT to 16:00 LT for the two cloud cover scenarios. Fig. 8 shows the occurrence frequency of low and high cloud covers from 10:00–16:00 LT in summer and winter seasons of the

years 1979–2014. As shown in Fig. 8a–b, the high cloud cover scenario occurred more frequently in summer, followed by the low cloud cover scenario. The occurrence frequency of high cloud cover during midday hours ranges from 0.53 to 0.82 and has no clear trend throughout the study period. In terms of the four nine-year periods, the occurrence frequency of high cloud cover has a slight upward trend in the first three periods then a decreasing trend in the last nine-year period. These occurrence frequency changes in high cloud cover cannot explain the significant increasing trend in temperature for the summertime high cloud cover scenario seen in Fig. 5b. Similarly, temporal temperature variations for low cloud cover scenario in summer cannot be interpreted as the result of the occurrence frequency changes in low cloud cover. As shown in Fig. 8c–d, there are no discernible trends in the occurrence frequencies of the two cloud cover scenarios during the study period. Therefore, cloud cover changes are not likely the reason for the temperature variation found in winter. However, it is worthy noting that changes in aerosol loading could affect the cloud properties including cloud cover (e.g., Zhang et al., 2010; Forkel et al., 2012). However, it is not discernible in our study and not considered here.

### 3.4. Contribution of aerosols to surface DSR and decadal temperature variability

The quantitative contribution of aerosol radiative forcing to atmospheric temperature during the study period can be estimated using the sensitivity of surface DSR to RH-corrected visibility (Fig. 6a and b) and  $\text{PM}_{2.5}$  (Fig. 6c and d). Based on the linear regression equation in Fig. 6b, the natural sensitivity of surface DSR to RH-corrected visibility is  $15.08 \text{ W m}^{-2} \text{ km}^{-1}$  in winter. According to the linear regression lines shown in Fig. 2, atmospheric visibility decreased from  $\sim 12 \text{ km}$  in the initial years of the study period to nearly  $12 \text{ km}$  in the last years of the study period. The average visibility decreased nearly  $2 \text{ km}$  over the study period. Based on these two parameters, the contribution of aerosols to surface DSR is  $\sim 30 \text{ W m}^{-2}$  over the 36 years studied. Note that the contribution of aerosols to surface energy includes the impacts from direct radiative forcing and from complicated aerosol-climate feedbacks. Assuming that the temperature differences in Fig. 3e are caused by the interaction between aerosols and surface DSR, the change in midday temperature relative to aerosol surface cooling is approximately  $2.1^\circ\text{C}$  during the last three nine-year periods. This temperature reduction is  $\sim 0.66^\circ\text{C}$  for all cloud cover scenarios. Note that this

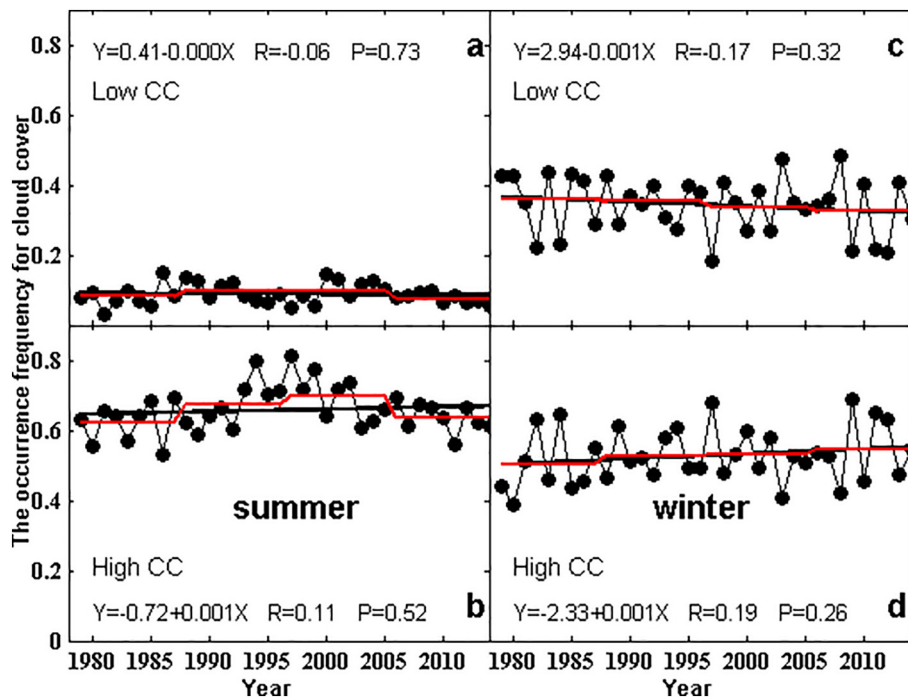


**Fig. 8.** Time series of the probability of occurrence of low cloud cover (CC, panels a and c), and high CC (panels b and d) from 1000 to 1600 Local Time. The left panels are for summer and the right panels are for winter. The black line through the points is the linear best-fit line. Connecting red lines show the trends in each of the four nine-year periods. (For interpretation of the references to colour in this figure legend, the reader is referred to the web version of this article.)

cooling could be offset to some degree by the impacts of GHGs and the urban heat island effect.

Wang and Dickinson (2013) estimated the contribution of changes in solar radiation to the decadal temperature variability using the formula  $0.5 \times \text{DTR}$  (the daily temperature range), which was established based on the relationship between radiation and DTR. According to their assumption that surface DSR does not change the daily minimum temperature, surface DSR reduces  $T_{\max}$  by  $\sim 0.4^{\circ}\text{C}$ . This estimated reduction in globally-averaged  $T_{\max}$  by surface DSR during the 1960s and 1970s is much lower than the value we obtained in Hong Kong during the midday hours under low cloud cover conditions ( $2.1^{\circ}\text{C}$ ) and even slightly lower than the value obtained when not considering cloud cover ( $0.66^{\circ}\text{C}$ ). The larger reduction in temperature associated with surface DSR in Hong Kong found in this study may be related to the heavy aerosol loading and the strong absorbing character of aerosols in this region.

The large negative aerosol forcing at the surface found in this study is consistent with many previous studies such as those from the Indian Ocean Experiment (INDOEX) (Ramanathan et al., 2001) and the East Asian Study of Tropospheric Aerosols: an International Regional Experiment (Li et al., 2007, 2010). Both showed a negative surface forcing in the order of  $-20 \text{ W m}^{-2}$  due to heavy pollution in south and east Asia. The strong surface cooling by aerosols is a dominating climate forcing agent in Asia which has contributed significantly to the changes of the monsoon climate in the region over the last a few decades (Li et al., 2016a, 2016b). This study helps us further understand the radiative effect of aerosol on temperature changes in a conjuncture zone affected both the eastern and southern monsoons that may have impeded upon the monsoon circulation and regional climate. Further studies are needed to investigate temperature changes at different altitudes induced by the inhomogeneous distribution and layers of aerosols which may have a strong feedback with the boundary-layer meteorology (Li et al., 2017).

#### 4. Summary

In recent decades, Hong Kong has experienced serious aerosol transport from the Pearl River Delta region of China, especially in winter. The contrast in aerosol loading and the consequent difference in

surface cooling between summer and winter could explain the distinct temperature variations between the two seasons observed in Hong Kong. Cloud fractions had no clear temporal trends in the summer and winter seasons of the study period (1979–2014) and are thus not likely a factor behind the different temperature trends seen in summer and winter. Our observational study shows a significant positive relationship between surface downwelling solar radiation (DSR) and atmospheric visibility, a consistent negative relationship between surface DSR and  $\text{PM}_{2.5}$  and a positive relationship between temperature and surface DSR. These relationships support a likely increasing trend in aerosol surface cooling effect observed in winter and a decreasing trend in summer in Hong Kong. Based on the linear regression analysis, the sensitivity of surface DSR to aerosol amount was  $\sim 15.08 \text{ W m}^{-2} \text{ km}^{-1}$ . The contribution of aerosols to midday surface DSR was estimated to be  $\sim 30 \text{ W m}^{-2}$  during the 36 winters (from 1979 to 2014) in Hong Kong, which could result in a reduction of about  $0.66^{\circ}\text{C}$  in midday temperatures ( $2.1^{\circ}\text{C}$  for the low cloud cover scenario only).

#### Acknowledgements

This work was supported by the Ministry of Science and Technology of China (2017YFC1501403), the National Natural Science Foundation of China (41575143 and 91544217), the State Key Laboratory of Earth Surface Processes and Resources Ecology (2017-KF-13), and the Fundamental Research Funds for the Central Universities (2017EYT18). Data used in this study are available upon request via email to Xin Yang (yangxin@bnu.edu.cn).

#### References

- Andreae, M.O., Schmid, O., Yang, H., Chand, D., Yu, J.Z., Zeng, L.M., Zhang, Y.H., 2008. Optical properties and chemical composition of the atmospheric aerosol in urban Guangzhou, China. *Atmos. Environ.* 42, 6335–6350. <http://dx.doi.org/10.1016/j.atmosenv.2008.01.030>.
- Cao, G., Zhang, X., Zheng, F., 2006. Inventory of black carbon and organic carbon emissions from China. *Atmos. Environ.* 40, 6516–6527. <http://dx.doi.org/10.1016/j.atmosenv.2006.05.070>.
- Cao, J.J., Lee, S.C., Chow, J.C., Watson, J.G., Ho, K.F., Zhang, R.J., Jin, Z.D., Shen, Z.X., Chen, G.C., Kang, Y.M., Zou, S.C., Zhang, L.Z., Qi, S.H., Dai, M.H., Cheng, Y., Hu, K., 2007. Spatial and seasonal distributions of carbonaceous aerosols over China. *J. Geophys. Res. Atmos.* 112, D22S11. <http://dx.doi.org/10.1029/2006JD008205>.
- Che, H.Z., Shi, G.Y., Zhang, X.Y., Arimoto, R., Zhao, J.Q., Xu, L., Wang, B., Chen, Z.H.,

2005. Analysis of 40 years of solar radiation data from China, 1961–2000. *Geophys. Res. Lett.* 32, L06803. <http://dx.doi.org/10.1029/2004GL022322>.
- Deng, X., Tie, X., Wu, D., Zhou, X., Bi, X., Tan, H., Li, F., Jiang, C., 2008. Long-term trend of visibility and its characterizations in the Pearl River Delta (PRD) region, China. *Atmos. Environ.* 42, 1424–1435. <http://dx.doi.org/10.1016/j.atmosenv.2007.11.025>.
- Dong, Z., Li, Z., Yu, X., Cribb, M.C., Li, X., Dai, J., 2017. Opposite long-term trends in aerosols between lower and higher altitudes: a testimony to the aerosol-PBL feedback. *Atmos. Chem. Phys.* 17, 7997–8009. <http://dx.doi.org/10.5194/acp-2017-2>.
- Du, C.L., Liu, S.Y., Yu, X., Li, X.M., Chen, C., Peng, Y., Dong, Y., Dong, Z.P., Wang, F.Q., 2013. Urban boundary layer height characteristics and relationship with particulate matter mass concentrations in Xi'an, central China. *Aerosol Air Qual. Res.* 13, 1598–1607.
- Forkel, R., Werhahn, J., Hansen, A.B., McKeen, S., Peckham, S., GRELL, G., Suppan, P., 2012. Effect of aerosol-radiation feedback on regional air quality - a case study with WRF/Chem. *Atmos. Environ.* 53, 202–211.
- Garland, R.M., Yang, H., Schmid, O., Rose, D., Nowak, A., Achtert, P., Wiedensohler, A., Takegawa, N., Kita, K., Miyazaki, Y., Kondo, Y., Hu, M., Shao, M., Zeng, L.M., Zhang, Y.H., Andreae, M.O., Pöschl, U., 2008. Aerosol optical properties in a rural environment near the mega-city Guangzhou, China: implications for regional air pollution, radiative forcing and remote sensing. *Atmos. Chem. Phys.* 8, 5161–5186.
- Garrett, T., Zhao, C., 2006. Increased Arctic cloud longwave emissivity associated with pollution from mid-latitudes. *Nature* 440, 787–789. <http://dx.doi.org/10.1038/nature04636>.
- Gong, D.Y., Guo, D., Ho, C.H., 2006. Weekend effect in diurnal temperature range in China: opposite signals between winter and summer. *J. Geophys. Res. Atmos.* 111, D18113. <http://dx.doi.org/10.1029/2006JD007068>.
- He, B., Bao, Q., Li, J., Wu, G., Liu, Y., Wang, X., Sun, Z., 2013. Influences of external forcing changes on the summer cooling trend over East Asia. *Clim. Chang.* 117. <http://dx.doi.org/10.1007/s10584-012-0592-4>.
- Huang, Y., Chameides, W.L., Dickinson, R.E., 2007. Direct and indirect effects of anthropogenic aerosols on regional precipitation over East Asia. *J. Geophys. Res. Atmos.* 112, D03212. <http://dx.doi.org/10.1029/2006JD007114>.
- IPCC, 2013. Climate change 2013. In: Stocker, T.F. (Ed.), *The Physical Science Basis. Contribution of Working Group I to the Fifth Assessment Report of the Intergovernmental Panel on Climate Change*. Cambridge University Press, Cambridge, United Kingdom and New York, NY, USA (1535 pp.). <https://doi.org/10.1017/CBO9781107415324>.
- Jacobson, M.Z., Kaufman, Y.J., 2006. Wind reduction by aerosol particles. *Geophys. Res. Lett.* 33, L24814. <http://dx.doi.org/10.1029/2006GL027838>.
- Jiang, J.H., Livesey, N.J., Su, H., Neary, L., McConnell, J.C., Richards, N.A.D., 2007. Connecting surface emissions, convective uplifting, and long-range transport of carbon monoxide in the upper troposphere: new observations from the Aura Microwave Limb Sounder. *Geophys. Res. Lett.* 34, L18812. <http://dx.doi.org/10.1029/2007GL030638>.
- Kaiser, D.P., Qian, Y., 2002. Decreasing trends in sunshine duration over China for 1954–1998: indication of increased haze pollution? *Geophys. Res. Lett.* 29 (21). <http://dx.doi.org/10.1029/2002GL016057>.
- Kaufmann, R.K., Kauppi, H., Mann, M.L., Stock, J.H., 2011. Reconciling anthropogenic climate change with observed temperature 1998–2008. *Proc. Natl. Acad. Sci. U. S. A.* 108 (29), 11790–11793. <http://dx.doi.org/10.1073/pnas.1102467108>.
- Kim, S.W., Choi, I.J., Yoon, S.C., 2010. A multi-year analysis of clear-sky aerosol optical properties and direct radiative forcing at Gosan, Korea (2001–2008). *Atmos. Res.* 95. <http://dx.doi.org/10.1016/j.atmosres.2009.10.008>.
- Li, Z., 1998. Influence of absorbing aerosols on the inference of solar surface radiation budget and cloud absorption. *J. Clim.* 11, 5–17.
- Li, Z., Xia, X., Cribb, M., Mi, W., Holben, B., Wang, P., Chen, H., Tsay, S.-C., Eck, T.F., Zhao, F., Dutton, E.G., Dickinson, R.E., 2007. Aerosol optical properties and their radiative effects in northern China. *J. Geophys. Res. Atmos.* 112, D22S01. <http://dx.doi.org/10.1029/2006JD007382>.
- Li, Z., Lee, K.-H., Xin, J., Wang, Y., Hao, W.-M., 2010. First observation-based estimates of aerosol radiative forcing at the top, bottom and inside of the atmosphere. *J. Geophys. Res. Atmos.* 115, D00K18. <http://dx.doi.org/10.1029/2009JD013306>.
- Li, Z., Lau, W.K.-M., Ramanathan, V., Wu, G., Ding, Y., Manoj, M.G., Liu, J., Qian, Y., Li, J., Zhou, T., Fan, J., Rosenfeld, D., Ming, Y., Wang, Y., Huang, J., Wang, B., Xu, X., Lee, S.-S., Cribb, M., Zhang, F., Yang, X., Zhao, C., Takemura, T., Wang, K., Xia, X., Yin, Y., Zhang, H., Guo, J., Zhai, P.M., Sugimoto, N., Babu, S.S., Brasseur, G.P., 2016a. Aerosol and monsoon climate interactions over Asia. *Rev. Geophys.* 54, 866–929. <http://dx.doi.org/10.1002/2015RG000500>.
- Li, Q., Zhang, R., Wang, Y., 2016b. Interannual variation of the wintertime fog-haze days across central and eastern China and its relation with east Asian winter monsoon. *Int. J. Climatol.* 36, 346–354.
- Li, Z., Guo, J., Ding, A., Liao, H., Liu, J., Sun, Y., Wang, T., Xue, H., Zhang, H., Zhu, B., 2017. Aerosols and boundary-layer interactions and impact on air quality. *Nat. Sci. Rev.* 4, 810–833. <http://dx.doi.org/10.1093/nsr/nwx117>.
- Liu, B., Xu, M., Henderson, M., Qi, Y., Li, Y., 2004. Taking China's temperature: daily range, warming trends, and regional variations, 1955–2000. *J. Clim.* 17, 4453–4462.
- Makowski, K., Jaeger, E.B., Chiachio, M., Wild, M., Ewen, T., Ohmura, A., 2009. On the relationship between diurnal temperature range and surface solar radiation in Europe. *J. Geophys. Res. Atmos.* 114, D00D07. <http://dx.doi.org/10.1029/2008JD011104>.
- Meehl, G.A., Washington, W.M., Wigley, T.M., Arblaster, J.M., Dai, A., 2003. Solar and greenhouse gas forcing and climate response in the twentieth century. *J. Clim.* 16, 426–444. [http://dx.doi.org/10.1175/1520-0442\(2003\)016<0426:SAGFA>2.0.CO;2](http://dx.doi.org/10.1175/1520-0442(2003)016<0426:SAGFA>2.0.CO;2).
- Qian, Y., Giorgi, F., 2000. Regional climatic effects of anthropogenic aerosols? The case of southwestern China. *Geophys. Res. Lett.* 27, 3521–3524.
- Qian, Y., Gong, D., Fan, J., Leung, L.R., Bennartz, R., Chen, D., Wang, W., 2009. Heavy pollution suppresses light rain in China: observations and modeling. *J. Geophys. Res. Atmos.* 114. <http://dx.doi.org/10.1029/2008JD011575>. D00K02.
- Qian, Y., Leung, R.L., Ghan, S.J., Giorgi, F., 2003. Regional climate effects of aerosols over China: modeling and observation. *Tellus B* 55 (4), 914–934. <http://dx.doi.org/10.1046/j.1435-6935.2003.00070.x>.
- Qian, Y., Kaiser, D.P., Leung, L.R., Xu, M., 2006. More frequent cloud-free sky and less surface solar radiation in China from 1955 to 2000. *Geophys. Res. Lett.* 33, L01812. <http://dx.doi.org/10.1029/2005GL024586>.
- Qian, Y., Wang, W.G., Leung, L.R., Kaiser, D.P., 2007. Variability of solar radiation under cloud-free skies in China: the role of aerosols. *Geophys. Res. Lett.* 34, L12804. <http://dx.doi.org/10.1029/2006GL028800>.
- Quan, J.N., Gao, Y., Zhang, Q., Tie, X.X., Cao, J.J., Han, S.Q., Meng, J.W., Chen, P.F., Zhao, D.L., 2013. Evolution of planetary boundary layer under different weather conditions, and its impact on aerosol concentrations. *Particuology* 11 (1), 34–40.
- Quan, J.N., Tie, X., Zhang, Q., Liu, Q., Li, X., Gao, Y., Zhao, D., 2014. Characteristics of heavy aerosol pollution during the 2012–2013 winter in Beijing, China. *Atmos. Environ.* 88, 83–89. <http://dx.doi.org/10.1016/j.atmosenv.2014.01.058>.
- Ramanathan, V., Crutzen, P.J., Lelieveld, J., Mitra, A.P., Althausen, D., Anderson, J., Andreae, M.O., Cantrell, W., Cass, G.R., Chung, C.E., Clarke, A.D., Coakley, J.A., Collins, W.D., Conant, W.C., Dulac, F., Heintzberg, J., Heymsfield, A.J., Holben, B., Howell, S., Hudson, J., Jayaraman, A., Kiehl, J.T., Krishnamurti, T.N., Lubin, D., McFarquhar, G., Novakov, T., Ogren, J.A., Podgorny, I.A., Prather, K., Priestley, K., Prospero, J.M., Quinn, P.K., Rajeev, K., Rasch, P., Rupert, S., Sadourny, R., Sathesh, S.K., Shaw, G.E., Sheridan, P., Valero, F.P.J., 2001. Indian Ocean Experiment: an integrated analysis of the climate forcing and effects of the great Indo-Asian haze. *J. Geophys. Res. Atmos.* 106 (D22), 28371–28398. <http://dx.doi.org/10.1029/2001JD900133>.
- Rosenfeld, D., Dai, J., Yu, X., Yao, Z., Xu, X., Yang, X., Du, C., 2007. Inverse relations between amounts of air pollution and orographic precipitation. *Science* 315 (5817), 1396–1398. <http://dx.doi.org/10.1126/science.1137949>.
- Shi, G.Y., Hayasaka, T., Ohmura, A., Chen, Z.H., Wang, B., Zhao, J.Q., Che, H.Z., Xu, L., 2008. Data quality assessment and the long-term trend of ground solar radiation in China. *J. Appl. Meteorol. Climatol.* 47, 1006–1016. <http://dx.doi.org/10.1175/2007JAMC1493.1>.
- Tang, W.-J., Yang, K., Qin, J., Cheng, C.C.K., He, J., 2011. Solar radiation trend across China in recent decades: a revisit with quality-controlled data. *Atmos. Chem. Phys.* 11, 393–406. <http://dx.doi.org/10.5194/acp-11-393-2011>.
- Tao, M., Chen, L., Wang, Z., Tao, J., Che, H., Wang, H., Wang, Y., 2015. Comparison and evaluation of the MODIS Collection 6 aerosol data in China. *J. Geophys. Res. Atmos.* 120, 6992–7005. <http://dx.doi.org/10.1002/2015JD023360>.
- Wang, K.C., Dickinson, R.E., 2013. Contribution of solar radiation to decadal temperature variability over land. *Proc. Natl. Acad. Sci. U. S. A.* 110 (14), 14877–14882. <http://dx.doi.org/10.1073/pnas.1311433110>.
- Wang, K., Dickinson, R.E., Liang, S., 2009. Clear sky visibility has decreased over land globally from 1973 to 2007. *Science* 323, 1468–1470. <http://dx.doi.org/10.1126/science.1167549>.
- Wang, Y., Wan, Q., Meng, W., Liao, F., Tan, H., Zhang, R., 2011. Long-term impacts of aerosols on precipitation and lightning over the Pearl River Delta megacity area in China. *Atmos. Chem. Phys.* 11 (12), 421–12,436. <http://dx.doi.org/10.5194/acp-11-12421-2011>.
- Wang, S., Xing, J., Zhao, B., Jang, C., Hao, J., 2014. Effectiveness of national air pollution control policies on the air quality in metropolitan areas of China. *J. Environ. Sci.* 26, 13–22. [http://dx.doi.org/10.1016/S1001-0742\(13\)60381-2](http://dx.doi.org/10.1016/S1001-0742(13)60381-2).
- Wang, Y., Jiang, J.H., Su, H., 2015. Atmospheric responses to the redistribution of anthropogenic aerosols. *J. Geophys. Res. Atmos.* 120. <http://dx.doi.org/10.1002/2015JD023665>.
- Wild, M., Ohmura, A., Makowski, K., 2007. Impact of global dimming and brightening on global warming. *Geophys. Res. Lett.* 34, L04702. <http://dx.doi.org/10.1029/2006GL028031>.
- Wu, D., Tie, X., Li, C., Ying, Z., Kai-Hon Lau, A., Huang, J., Deng, X., Bi, X., 2005. An extremely low visibility event over the Guangzhou region: a case study. *Atmos. Environ.* 39, 6568–6577. <http://dx.doi.org/10.1016/j.atmosenv.2005.07.061>.
- Wu, Y., Zhu, J., Che, H., Xia, X., Zhang, R., 2015. Column-integrated aerosol optical properties and direct radiative forcing based on sun photometer measurements at a semi-arid rural site in Northeast China. *Atmos. Res.* 17, 56–65. <http://dx.doi.org/10.1016/j.atmosres.2015.01.021>.
- Xia, X., 2012. Significant decreasing cloud cover during 1954–2005 due to more clear sky days and less overcast days in China and its relation to aerosol. *Ann. Geophys.* 30, 573–582. <http://dx.doi.org/10.5194/angeo-30-573-2012>.
- Xia, X., Wang, P., Chen, H., Liang, F., 2006. Analysis of downwelling surface solar radiation in China from National Centers for Environmental Prediction reanalysis, satellite estimates, and surface observations. *J. Geophys. Res. Atmos.* 111 (D09103). <http://dx.doi.org/10.1029/2005JD006405>.
- Yang, X., Dong, W., Liu, F., 2011. Impact of air pollution on summer surface winds in Xi'an. *Acta Meteor. Sin.* 25 (4), 527–533. <http://dx.doi.org/10.1007/S13351-011-0411-2>.
- Yang, X., Yao, Z., Li, Z., Fan, T., 2013a. Heavy air pollution suppresses summer thunderstorms in central China. *J. Atmos. Sol.* 95–96, 28–40. <http://dx.doi.org/10.1016/j.jastp.2012.12.023>.
- Yang, X., Ferrat, M., Li, Z., 2013b. New evidence of orographic precipitation suppression by aerosols in central China. *Meteorog. Atmos. Phys.* 119, 17–29. <http://dx.doi.org/10.1007/s00703-012-0221-9>.
- Yang, X., Zhao, C., Guo, J., Wang, Y., 2016a. Intensification of aerosol pollution associated with its feedback with surface solar radiation and winds in Beijing. *J. Geophys. Res. Atmos.* 121, 4093–4099. <http://dx.doi.org/10.1002/2015JD024645>.

- Yang, X., Zhao, C., Zhou, L., Wang, Y., Liu, X., 2016b. Distinct impact of different types of aerosols on surface solar radiation in China. *J. Geophys. Res. Atmos.* 121, 6459–6471. <http://dx.doi.org/10.1002/2016JD024938>.
- Yuan, Z.B., Yu, J.Z., Lau, A.K.H., Louie, P.K.K., Fung, J.C.H., 2006. Application of positive matrix factorization in estimating aerosol secondary organic carbon in Hong Kong and its relationship with secondary sulfate. *Atmos. Chem. Phys.* 6, 25–34. <http://dx.doi.org/10.5194/acp-6-25-2006>.
- Zhang, Y., Wen, X.Y., Jang, C.J., 2010. Simulating chemistry-aerosol-cloud-radiation-climate feedbacks over the continental U.S. using the online-coupled Weather Research Forecasting Model with chemistry (WRF/Chem). *Atmos. Environ.* 44, 3568–3582.
- Zhao, C., Garrett, T., 2015. Effects of Arctic haze on surface cloud radiative forcing. *Geophys. Res. Lett.* 42. <http://dx.doi.org/10.1002/2014GL062015>.
- Zhao, B., Wang, S., Wang, J., Fu, J.S., Liu, T., Xu, J., Fu, X., Hao, J., 2013. Impact of national NO and SO control policies on particulate matter pollution in China. *Atmos. Environ.* 77, 453–463. <http://dx.doi.org/10.1016/j.atmosenv.2013.05.012>.